

# Online NMR Flowing Fluid Measurements

Feng Deng<sup>1</sup> · Lizhi Xiao<sup>2</sup> · Mengying Wang<sup>1</sup> ·  
Ye Tao<sup>1</sup> · Lulin Kong<sup>1</sup> · Xiaoning Zhang<sup>1</sup> ·  
Xinyun Liu<sup>1</sup> · Dongshi Geng<sup>1</sup>

Received: 1 June 2016 / Revised: 12 August 2016 / Published online: 6 October 2016  
© Springer-Verlag Wien 2016

**Abstract** Online nuclear magnetic resonance (NMR) is an efficient fluid detection method for fluid flowing measurement. In our previous work, the velocity effects on the motion NMR measurement were studied and the velocity correction method was proposed. However, the flow state effects on NMR measurement is more complicated than motion velocity effects. Thus, the influence of flow state on NMR measurement is investigated. A multi-functional low-field and online NMR fluid analysis system is developed to realize the rapid measurement of one-dimensional and two-dimensional NMR relaxation times of fluids under slow laminar flow state.

## 1 Introduction

As an efficient, nondestructive detection technology for porous media, fluid, and gas, online nuclear magnetic resonance (NMR) has been widely applied in a variety of disciplines, such as physics, chemistry, biology, medicine, agriculture, and geology, all of which have real-time demand. In contrast to traditional low-field NMR under static measurement mode, online detection techniques are faced with many challenges. Instruments that are used for static detection cannot be directly exploited for online measurement.

There are two modes of online NMR detection. One is stationary sample with probe motion, which can be used to detect large objects, such as well logging [1], online scanning of building material [2] and soil moisture [3]. The other is stationary

---

✉ Feng Deng  
dengfeng0719@petrochina.com.cn

<sup>1</sup> The Research Institute of Petroleum Exploration and Development, China National Petroleum Corporation (CNPC), 20# Xueyuan Road, Beijing 100083, People's Republic of China

<sup>2</sup> State Key Laboratory of Petroleum Resources and Prospecting, China University of Petroleum, Beijing 102249, People's Republic of China

probe with the motion of sample, which can be applied to the detection of the fluid flow in real time [4, 5], such as the flowing blood measurements [6], online detection of transport pipeline of gas or liquid, monitoring of chemical reaction processes, etc. In the first detection mode, the measurement responses are mainly affected by velocity, while the second one is influenced by both measurement velocity and the flow characteristic of the fluid sample. For the first mode, to eliminate the velocity effects on polarization and echo acquisition process of NMR measurement, our previous work has presented a set of motion correction method, and in performance work we have proposed motion correction method [7]. This paper is a supplement to the previous work and mainly focuses on the second detection mode.

In this research on the effects of flow state on NMR measurement, a multi-functional low-field and online NMR fluid analysis system is developed, which can realize measurements of NMR relaxation times of a continuous fluid flow.

## 2 Flowing Effects on Online NMR Measurements

Remarkable distinctions exist between online NMR measurement of fluid static and flow measurement of fluid. The fluid molecules in the detection region of the NMR probe experience Brownian motion under stationary measurement state, in which the sample has sufficient polarization time. In addition, the fluid does not change much in the process of collecting echo signals and transmitting pulse sequences within the detection area. However, flowing fluid sample may not have sufficient time to experience complete polarization in the motion state NMR measurement because of the flow rate, as shown in Fig. 1. In the process of transmitting pulse sequences and collecting echoes, the fluid in the area of detection is constantly changing, which inevitably leads to signal loss during acquisition.

For performance evaluation, we have analyzed the motion effects of well logging in an oil industry and proposed motion correction method [7]. Notably, wireline NMR logging is achieved by acquiring NMR signal with the continuous motion of probe and static detected sample. As such, the sample and probe are in translational motion, which is different from online measurement of flowing fluid (Fig. 1). The rheological property of laminar flow fluid indicates the existence of an army of flow mode, such as Bingham model [8], Ostwald-de Waele power law model, Casson model [9], Herschel–Bulkley (H-B) model [10], and Robertson–Stiff (R-S) model [11], under the same differential pressure. The fluid of the same flow mode has different status, including plug flow, laminar flow, and turbulent flow.

In plug flow mode, the flow velocity effects on NMR measurement are the same as that on a probe motion and a static sample; the expressions are as follows:

$$\text{ECHO} = \begin{cases} M_i = S_i H_{1,i} \left\{ 1 - \exp \left[ -\text{TW} \left( \frac{1}{T_{1,i}} + X_v \right) \right] \right\} \\ \sum_{i=1}^n M_i \exp \left[ -t \left( \frac{1}{T_{2,i}} + Y_v \right) \right], & t < \frac{L_A}{v} \\ 0, & t \geq \frac{L_A}{v} \end{cases}, \quad (1)$$

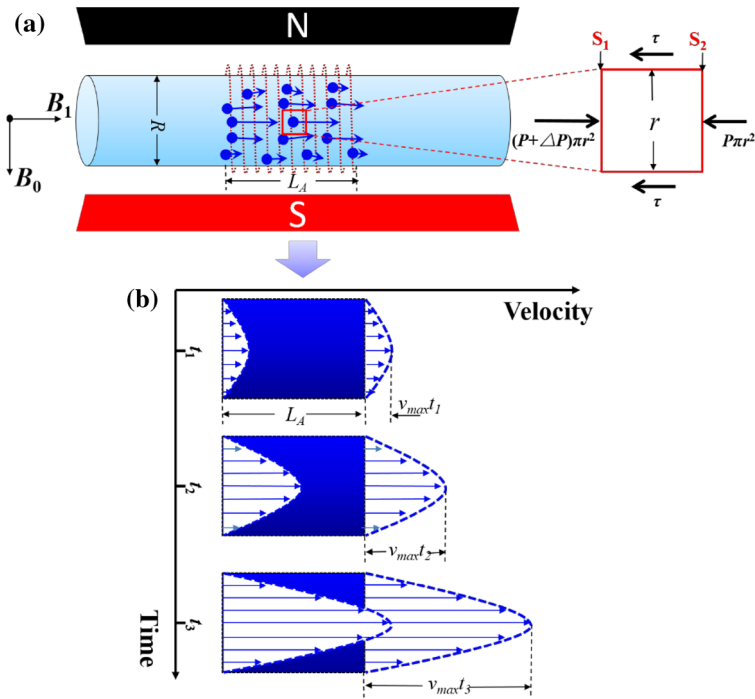


**Fig. 1** Molecular motion state diagram of a fluid under flowing state

where  $M_i$  is the signal intensity of different fluids after polarization, ECHO is the collected echo signal with the Carr–Purcell–Meiboom–Gill (CPMG) pulse sequence at time  $t$ ,  $S_i$  and  $H_{1,i}$  express the saturation and hydrogen index of the fluid,  $T_{1,i}$  and  $T_{2,i}$  denote the longitudinal and transverse relaxation times of different components, respectively, TW is the polarization time,  $L_A$  is the length of antenna,  $v$  is flow velocity,  $X_v$  and  $Y_v$  represent flow effects of the polarization and echo acquisition processes, respectively; the expressions are shown in [7]. In other flow mode, the situation is different.

This paper studies the steady flow fluid (accelerated speed = 0) and incompressible fluid in cylindrical coordinates using the force balance analysis method. As shown in Fig. 1a, for the radius as  $R$  and length as  $L_A$  cylindrical, due to the steady flow of fluid in a circular tube, acting on a fluid element must maintain the balance of force. The external forces acting on it are: the pressure on the fluid element left side section  $S_1$  is  $(P + \Delta P)\pi r^2$ , same with the flow direction; the pressure on the fluid element right side section of  $S_2$  is  $P\pi r^2$ , opposite with the flow direction; the total force is  $\Delta P\pi r^2$ , the same with the flow direction. Due to the fluid element which moves faster than the outer side of the fluid, Therefore, in vitro side of element receives a shear stress on the role of  $\tau$  with an opposite the flow direction, so the fluid outside the side face of resistance is  $2\pi r^2 L_A$ . The fluid force balance can be obtained:

$$\Delta P \pi r^2 = 2 \pi r L_A \tau, \tag{2}$$

where  $\Delta P$  is the fluid pressure difference at both sides of the pipe in the detection range and  $r$  is in range of  $0-R$ ,  $R$  is the diameter of fluid tube; the shear stress  $\tau$  is:

$$\tau = \frac{\Delta P r}{2 L_A} = -\eta \frac{du}{dr}, \tag{3}$$

where  $\eta$  is the plastic viscosity and  $u$  is the average flow velocity. By combining Eqs. 2 and 3, we obtain:

$$du = -\frac{\Delta P}{2 \eta L_A} r dr. \tag{4}$$

Then, the velocity distribution on the transverse section is determined as:

$$v(r) = \frac{Q(r)}{\pi R^2} = \frac{\Delta P}{4 \mu L_A} (R^2 - r^2), \tag{5}$$

where  $Q$  is the rate of flow and  $R$  is the diameter of sample tube. The velocity distributions under other flow modes are shown in Sect. 6. The general expressions of  $X_v$  and  $Y_v$  are as follows:

$$\begin{aligned} X_{v,1} &= \int_0^R X_{v,1}(r) dr = \int_0^R \left( \frac{L_M}{v(r)TW} - \frac{1}{T_{1,i}} \right) dr \\ X_{v,2} &= \int_0^R X_{v,2}(r) dr = \int_0^R \left\{ \begin{array}{ll} -\frac{1}{TW} \ln \left( 1 - \frac{v(r)TW}{L_A} \right) \approx \frac{v(r)}{L_A}, & v(r)TW < L_A \\ +\infty & , v(r)TW \geq L_A \end{array} \right\} dr \\ Y_v &= \int_0^R Y_v(r) dr = -\int_0^R \frac{1}{t} \ln \left( 1 - \frac{v(r)t}{L_A} \right) dr \approx \int_0^R \frac{v(r)}{L_A} dr, \end{aligned} \tag{6}$$

where  $L_M$  is the length of pre-polarization magnet,  $X_{v,1}$  and  $X_{v,2}$  represent flow velocity caused by ‘less-polarization’ and ‘over-polarization’ phenomena, respectively.

Figure 2 illustrates the simulation of the influence of flow state of different fluid mode on NMR measurements, with the same average flow velocity  $u$  and homogenous  $B_0$  and  $B_1$ .

The simulation result shows that the effects of plug flow and laminar flow with the same velocity on  $T_2$  spectrum are almost the same, with similar migration from the static spectrum. Therefore, to analyze the effects of flow velocity on the measurement of NMR relaxation times, all of the flow modes can be considered as plug flow with the same average velocity, thus, velocity correction method is applied. The application of flow velocity correction method requires an acquisition signal loss degree of <10 % [12]. To achieve this requirement, on the one hand, sufficient polarization time is needed for a fluid to flow through the pre-polarized

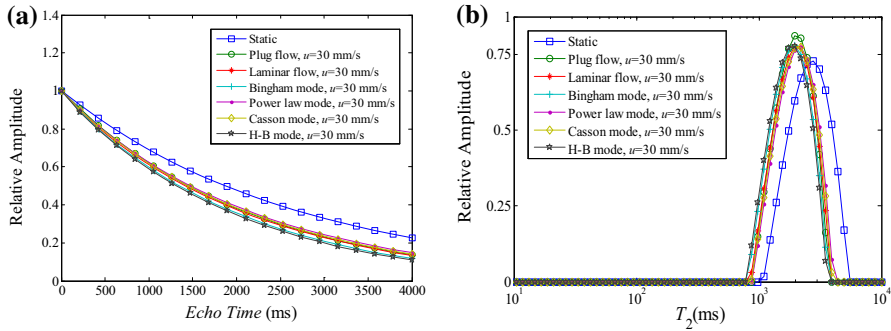


**Fig. 2** Flowing effect on NMR measurement

magnet area, thus, a longer pre-polarized magnet is necessary; on the other hand, longer antenna and large detection zone are needed to reduce the signal loss caused by the flow velocity during the signal acquisition time. This paper focuses on the design of an online NMR fluid analysis probe to increase the polarization efficiency and reduce signal loss.

### 3 Device

To realize the online NMR fluid measurement, we developed a set of multi-functional low-field and online NMR fluid analysis system (Fig. 3) [13, 14]. This system consists of three parts: a spectrometer and a programmable logic controller (PLC), a sampling control system, and a probe. The spectrometer system comprises analog and digital circuits, which were developed by our group [15]. The Siemens S7-200 PLC is used to control the pump, and thus the flow rate. The sampling control system is composed of an adjustable flow rate pump to maintain a continuous flow of fluid through the probe. The probe consists of a magnet and an antenna, as shown in Fig. 3.

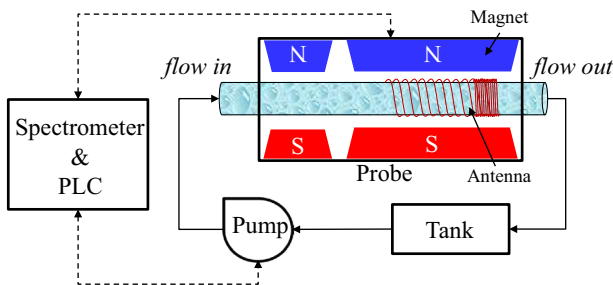


**Fig. 3** Schematic diagram of a low-field online NMR fluid analysis system

### 3.1 Magnet

It is very inefficient to directly use objective magnetization vector of pre-polarized magnet for fluid samples during the polarization process which requires longer pre-polarized magnet while the faster the flow rate is the longer the pre-polarized magnet requires. There are two schemes that can remove the effects on NMR measurement which caused by incomplete polarization. One scheme is to do motion corrections for obtained echo sequences; another scheme is to eliminate motion effects by designing the magnet structure of the probe.

This paper describes a multi-stage magnetic structure (shown as Fig. 4a) so that it can effectively solve the problem of polarization time which is not sufficient. The structure is a combination of two magnet structures with different field strength, respectively, and an air section which has certain thickness, meanwhile, the magnet of section A and the air of section B make up polarization area of the probe, magnet of section C is a detection area. All magnets adopt the circular structure, the polarization direction is along the Z-axis as shown in Fig. 4a. The parameters of size and field strength of the three-stage structure is shown in Table 1. In practical measurements, the fluid flows into the first magnet section A for polarization, the magnet field strength of the center of section A is higher than the central detection region (as shown in Fig. 4b) of section C, the purpose of which is to rapidly polarize the samples and make the magnetization vector after samples go through the magnet of section A that is higher than objective magnetization vector of detection area; the purpose of B is to use air to rapidly ‘drop down’ the magnetization vector after ‘hyperpolarized’ by magnet of section A to make them close to the objective magnetization vector when they enter into detection area of section C. The length of

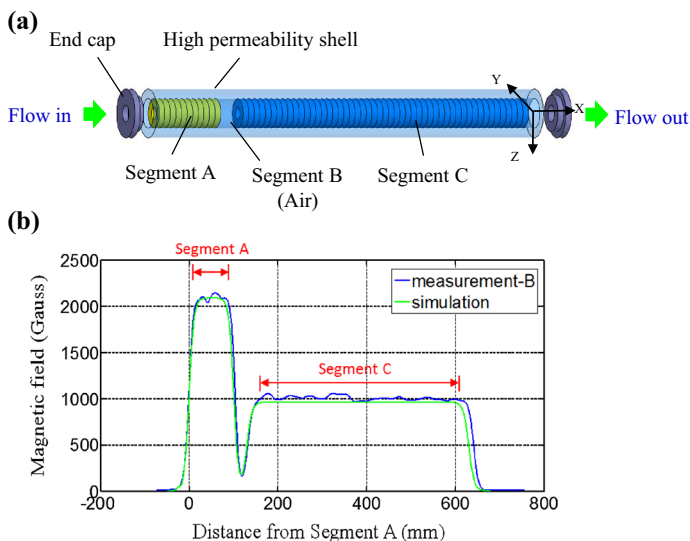


**Fig. 4** The two magnetic structure probe. **a** Magnetic structure diagram; **b** the intensity of static magnetic field on the central axis of the probe

**Table 1** Relative size parameters of two magnetic structure probe

|           | Material        | Length (mm) | Probe diameter (mm) | Thickness of high permeability shell (mm) | Thickness of magnets (mm) | Center field (Gauss) |
|-----------|-----------------|-------------|---------------------|---|---------------------------|----------------------|
| Segment A | Samarium cobalt | 109         | 80                  | 19  | 12.6                      | 2094                 |
| Segment B | Air             | 30          | 80                  | 19  |                           |                      |
| Segment C | Ferrite         | 510         | 80                  | 16  | 14                        | 966                  |

section A and B is a critical fact to decide whether the fluids will reach to objective magnetization vector after entering into detection zone or not, it is necessary to analysis the magnetization vector about the fluids after going through section A and B to study whether it could reach to magnetization vector detection range (less than 5 %) or not. Equation 7 gives a variation of magnetization vector  $M(t)$  as the fluids flow into the pre-polarization region of the probe at time  $t$ :

$$M(t) = M_A(1 - e^{-t_1/T_1})e^{-(t-t_1)/T_1}, \tag{7}$$

where,  $t_1 = L_A/v$  and  $L_A$  is the length of section A magnet,  $v$  is the velocity of flow,  $M_A$  is field strength of section A magnet. The options of field strength of section A magnet and length of section A and B need to observe the following two principles: (1) ensuring that the magnetization vector will be close to the area magnetization vector after the fluids which have more larger  $T_1$  range flowing through the pre-polarized magnet at more faster flow rate. (2) pre-polarized magnet need to be as short as possible to reduce the overall length and weight of the probe. As shown in Fig. 5. Under premise that the length of section B air zone and flow rate of fluids is fixed at 30 mm and 30 mm/s, respectively, the variance is the deviation between objective magnetization vector and magnetization vector which is obtained when fluids that contain different  $T_1$  components under the condition of different length of section A magnet are enter into detection area at 30 mm/s flow rate (the allowed maximum flow rate of designed system). It will be decided through the numerical simulation that when  $A = 109$  mm,  $B = 30$  mm, even though the variation of  $T_1$

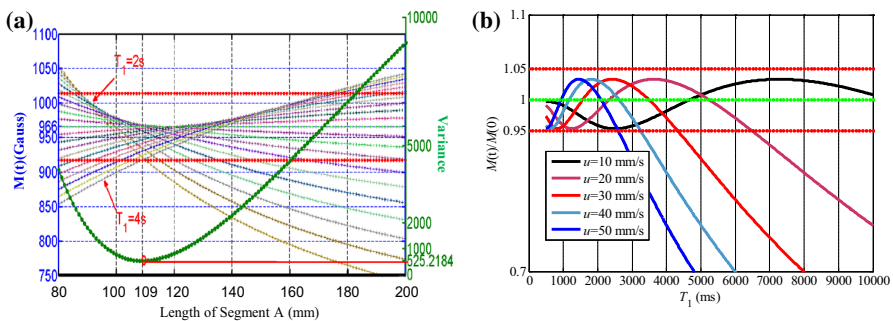


**Fig. 5** Numerical simulation of the magnetic vector of fluid flow in the detection area of section C. **a** Numerical simulation of magnetic vector of fluid that has different  $T_1$  components with different magnet lengths of section A (the velocity of the fluid is 3 cm/s); **b** magnetization of different  $T_1$  components of the fluid after flowing through the pre-polarization magnets at different speeds

range is larger, it still can ensure that fluids enter the detection area reaching objective magnetization vector.

### 3.2 Separated Antenna

As the same effect as insufficient polarization caused by NMR measurements, the insufficiency of signal acquisition can be suppressed using two schemes, one is still the movement velocity correction; another is the design of separate antenna structure aimed at NMR online measurement, as shown in Fig. 6. Separate antenna is placed at the end of detection area of C section magnet, it has changed the traditional NMR instrument that contains “single-input single” antenna structure. Its structure contains longer antennas which used to transmit pulse sequence, and a reception antenna which is parallel to transmitting antennas to receive echo signal, the purpose of this design is to offset effects of certain part of flow velocity. Using CPMG pulse sequence for example, CPMG pulse sequence comprises a series of  $90^\circ$  and  $180^\circ$  pulse. If using the separate antenna structure to do measurements with CPMG pulse sequence, fluids within the transmitting antenna  $A_1$  region will be excited by  $90^\circ$  pulse at first, only the echo signal can be received in the antenna  $A_2$  section in the subsequent process of collecting echo signals, therefore, during a CPMG pulse sequence, as long as fluid flows through the length of the distance  $S \leq A_1 - A_2$ , then the flow rate cannot theoretically affect the NMR signal acquisition.

In this paper, transmitting antenna of online NMR fluid analysis system  $A_1 = 300$  mm, receiving antenna  $A_2 = 30$  mm, the inner diameter of sample tube is 10 mm, allowed maximum detectable velocity is 30 mm/s.

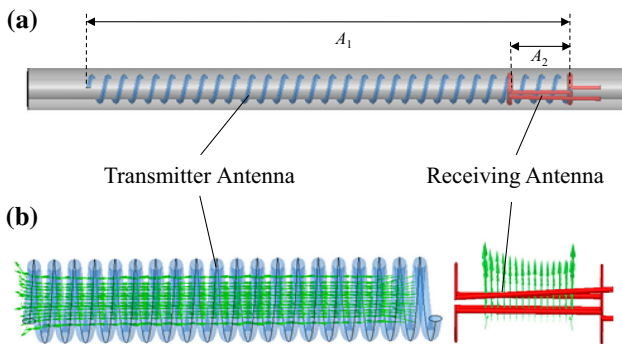


**Fig. 6** Schematic of separate antenna structure and RF field direction. **a** The lengths of transmitting antenna ( $A_1$ ) and the receiving antenna ( $A_2$ ) are 300 and 30 mm, respectively. **b** Direction of RF magnetic field of the separate antennas, the *green arrow* shows the numerical simulation of the two-antenna RF field direction, the directions of the RF field of these antennas are orthogonal to avoid interference coupling

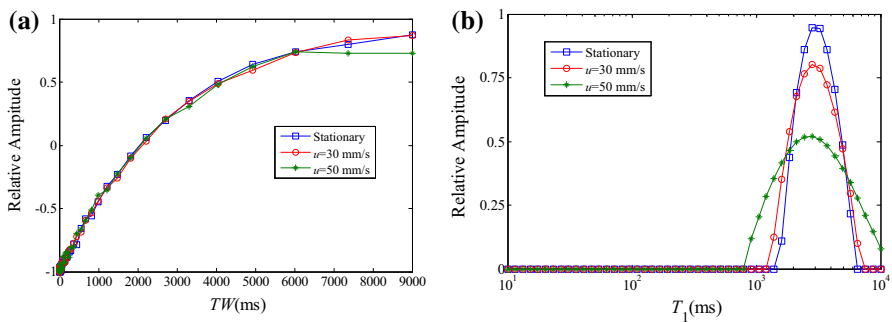


### 4 Experiments

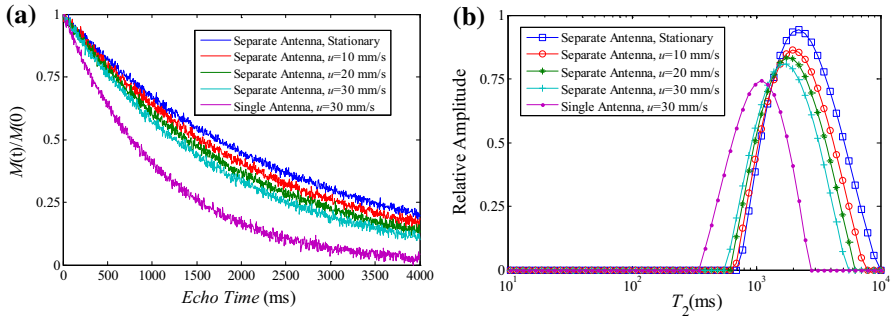
Flow measurement experiment was conducted in a laboratory environment using a multi-functional low-field and online NMR fluid analysis system. The sample is distilled water. Using inversion recovery (IR) and CPMG pulse sequences to measure the NMR relaxation times of distilled water under different flow velocities, and then the  $T_1$ - $T_2$  distributions were obtained by Laplace transform inversion. Experimental parameters are as follows, echo interval time  $T_E = 2$  ms, the TW values are selected in the range of  $0.5\text{--}9 \times 10^3$  ms logarithmically. Other experimental parameters are show in the figure legend.

Figure 7 shows the FID signal and inversion results of distilled water obtained by IR pulse sequence under different flow velocities; the experimental parameters as shown in the figure note. The results show that the multi-segment magnetic structure can increase the polarization efficiency. At 0–50 mm/s velocity, the distilled water samples were completely polarized before flowing into the detection region (the value of magnetization vector tipped by  $180^\circ$  pulse of IR pulse sequence is  $-M(0)$ ); the double-antenna structure provides plenty of recovery times (of 0–30 mm/s) for the magnetization of flow sample under the velocity range. Thus, this magnetic structure can eliminate the flow effects on  $T_1$  measurement.

Figure 8 shows the  $T_2$  experiment results obtained by CPMG pulse sequence. The results show that the use of separate antenna structure can reduce the flow effect on  $T_2$  map, but such effect cannot be completely eliminated. In addition, as shown in Fig. 8a, faster velocity results in larger influence, because the physical properties of the fluid flow may change. Flow can conceal the effect of Brownian motion of a fluid, which results in the enlargement of diffusion coefficient. This phenomenon directly affects the measurement result of  $T_2$ . For these effects, on the one hand, the homogeneity of static magnetic field of the detection region can be improved (the sample tube diameter decreases or the magnet structure optimization) or the flow rate can be decreased. On the other hand, the DEFSR and DEFIR pulse sequences for rapid measurement of 2D relaxation times are proposed in our performance work



**Fig. 7** Analysis of distilled water samples using IR pulse sequence. The experimental parameters are as follows: the polarization time TW values are selected in the range of  $0.5\text{--}9 \times 10^3$  ms logarithmically, to collect FID signal; the experiments were repeated in static, 3 and 5 cm/s. **a** First amplitude of FID signal; **b**  $T_1$  maps



**Fig. 8** Analysis of distilled water samples using CPMG pulse sequence. The experimental parameters are as follows:  $TW = 0$  (polarization was completed after the fluid flows through the pre-polarized magnet), echo interval time  $T_E = 2$  ms, number of echoes  $N = 2000$ ; the experiments were repeated in static, 10, 20 and 30 mm/s, and a single antenna (using the transmit antenna of separate antenna as a transmit and receive antenna) was used to collect echo train under 3 cm/s, separately. **a** Echo signal collected by CPMG pulse sequence; **b**  $T_2$  maps

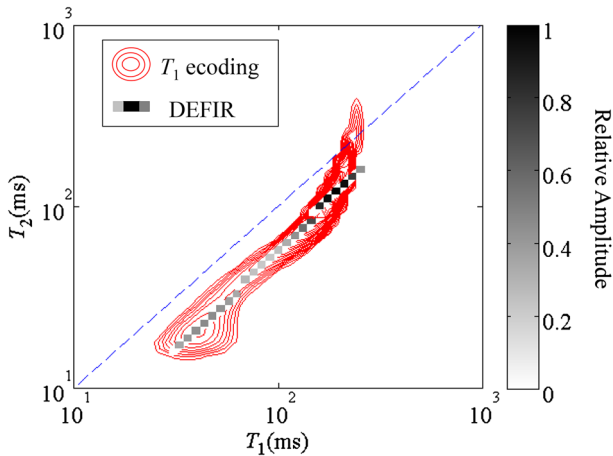


**Fig. 9** 2D distribution of the relaxation times of a light oil sample obtained by DEFIR pulse sequence measurements. The red equipotential line represents the  $T_1$ - $T_2$  distribution obtained by  $T_1$  echo pulse sequence, the solid line represents the  $T_1$ - $T_2$  distribution obtained by DEFIR sequence measurement. The experimental parameters are as follows:  $TW_{FIR}$  values were selected in the range of 0.5–300 ms logarithmically, the one sample measuring time by DEFIR pulse sequence with these parameters is about 40 ms; The traditional pulse sequence measured parameters: echo spacing  $T_E = 0.2$  ms, number of echoes  $N = 2000$ , polarization time  $TW$  values were selected in the range of 0.5–1500 ms logarithmically

[16, 17]. Given that these two pulse sequences are mainly applicable to  $T_1$  measurement, which is insensitive to molecular diffusion, the accurate measurement of fluid relaxation times at the flowing state is implemented to apply the two pulse sequences on the multi-functional low-field and online NMR fluid analysis system. As shown in Fig. 9, for flow measurements of light oil sample ( $\eta$  is 210.4 mPa s at 20 °C), the 2D  $T_1$ - $T_2$  distributions measured by DEFIR pulse sequence are in good agreement with that measured by  $T_1$ -encoding pulse sequence [18].

## 5 Conclusion

The on-site and real-time NMR measurement method is an efficient detection mode for flowing fluid. However, the flow state affects the NMR measurement in two aspects:

1. Flow velocity effects. Theoretical analysis and experimental verification show that the influence of flow velocity can be eliminated using the following two methods: (a) motion correction, in which the collected signals measured by IR and CPMG pulse sequence are corrected, but a longer polarization magnet and an antenna are needed to make up for the insufficient polarization and acquisition signal loss; (b) use of multi-magnetic and separate antenna structure, this probe optimization method can make up for the limitation of the first method by decreasing polarization time without motion correction.
2. For the inhomogeneity of  $B_0$  and  $B_1$  fields, the apparent diffusion coefficient increases under flow state; the experimental results show that using multi-magnetic and separate antenna structure, the rated flow velocity almost has no effect on the  $T_1$  measurement, and the effect on  $T_2$  measurement is reduced. By combining the DEFIR pulse sequence, the measurement of  $T_2$ , which is quite sensitive to molecular diffusion, is replaced by that of  $T_1$ , which is insensitive to molecular diffusion. By adopting this pulse sequence on the multi-functional low-field and online NMR fluid analysis system can be used for flowing fluid measurement.

**Acknowledgments** This work was supported by the National Science and Technology Major Project of the Ministry of Science and Technology of China (2016ZX05031-001) and National Scientific Instrument Development Project (21427812).

## Appendix: The Flow Velocity Distributions in Circular Tube Under Different Flow Patterns

(1) Bingham model [8].

Bingham mode velocity distribution function  $v(r)_b$ :

$$v(r)_b = \left\{ \begin{array}{ll} \frac{\Delta P_b}{4\eta_p L_A} (R - r)^2, & r \leq r_m \\ \frac{\Delta P_b}{4\eta_p L_A} [(R - r_m)^2 - (r - r_m)^2], & r > r_m \end{array} \right\}, \tag{8}$$

where  $\Delta P_b$  is the Bingham mode fluid pressure difference at both sides of the pipe in the detection range:

$$\Delta P_b = \frac{8\eta_p L_A u}{R^2} + \frac{8\tau_0 L_A}{3R}, \tag{9}$$

$L_A$  is the length of antenna,  $R$  is the diameter of the sample tube,  $\eta_p$  is the plastic viscosity of Bingham mode fluid:

$$\eta_p = 300 \frac{\theta_2 - \theta_1}{N_2 - N_1}, \quad (10)$$

$\theta_1$ ,  $\theta_2$  represent the rheological coefficients is in rotary viscometer's rotor with rotation rate  $N_1$ ,  $N_2$ , respectively,  $\tau_0$  is the yield value:

$$\tau_0 = \frac{K_\tau(\theta_1 N_2 - \theta_2 N_1)}{B_b(N_2 - N_1)}, \quad (11)$$

the constant  $K_\tau$  is determined by rotary viscometer inner cylinder size and the characteristics of the spring,  $B_b$  is the Bingham fluid correction coefficient:

$$B_b = \frac{2R_0^2}{R_0^2 - R_i^2} \ln \frac{R_0}{R_i}, \quad (12)$$

$R_0$ ,  $R_i$  represent the rotary viscometer's outer and inner tube diameter, the flow core radius:

$$r_m = \frac{2L_A \tau_0}{\Delta P}. \quad (13)$$

(2) Ostwald-de Waele power law model.

Power law mode velocity distribution function  $v(r)_p$ :

$$v(r)_p = \frac{n}{n+1} \left( \frac{\Delta p_p}{2KL_A} \right)^{\frac{1}{n}} \left( R^{\frac{n+1}{n}} - r^{\frac{n+1}{n}} \right), \quad (14)$$

where  $\Delta P_p$  is the Power law mode fluid pressure difference at both sides of the pipe in the detection range:

$$\Delta P_p = \frac{2KA}{R} \left( \frac{3n+1}{4n} \right)^n \left( \frac{4u}{R} \right)^n, \quad (15)$$

$n$  is the liquidity index:

$$n = \frac{\lg(\theta_2/\theta_1)}{\lg(N_2/N_1)}, \quad (16)$$

$K$  is the viscosity coefficient:

$$K = \frac{0.511\theta_{600}}{(1022B_p)^n}, \quad (17)$$

$B_p$  is Power law mode fluid correction coefficient:

$$B_p = \frac{(R_i/R_0)^2 - 1}{n[(R_i/R_0)^{2/n} - 1]}. \quad (18)$$

(3) Casson model [9].

Casson mode velocity distribution function  $v(r)_c$ :

$$v(r)_c = \frac{1}{\eta_k} \left[ \frac{\Delta P_c}{4L_A} (R^2 - r^2) - \frac{4}{3} \tau_c^{0.5} \left( \frac{\Delta P_c}{2L_A} \right)^{0.5} (R^{1.5} - r^{1.5}) + \tau_c (R - r) \right], \tag{19}$$

where  $\Delta P_c$  is the Casson mode fluid pressure difference at both sides of the pipe in the detection range:

$$\Delta P_c = \left[ \frac{2A}{R} \left( \frac{4\eta_k u}{R} - \frac{4}{147} \tau_c \right)^2 + \frac{8}{7} \tau_c^{0.5} \right]^2, \tag{20}$$

$\eta_k$  is the plastic viscosity of Casson mode fluid:

$$\eta_k = \left[ \frac{\sqrt{K_\tau}(\sqrt{\theta_2} - \sqrt{\theta_1})}{\sqrt{K_\gamma}(\sqrt{N_2} - \sqrt{N_1})} \right]^2, \tag{21}$$

$K_\gamma$  according to the rotary viscometer’s outer and inner tube diameter,  $B_c$  is Casson mode fluid correction coefficient:

$$B_c = 2 \frac{R_0}{R_0 + R_i}, \tag{22}$$

$\tau_c$  is the Casson yield value:

$$\tau_c = \left[ \frac{\sqrt{K_\tau}(\sqrt{\theta_1 N_2} - \sqrt{\theta_2 N_1})}{B_c(\sqrt{N_2} - \sqrt{N_1})} \right]^2. \tag{23}$$

(4) Herschel–Bulkley model [10]

H-B mode velocity distribution function  $v(r)_h$ :

$$v(r) = \frac{n}{n + 1} \left( \frac{\Delta P_h}{2KA} \right)^{\frac{1}{n}} \left[ (R - r_m)^{\frac{n+1}{n}} - (r - r_m)^{\frac{n+1}{n}} \right], \tag{24}$$

make the coefficients  $a = \theta_{600} - \theta_{300}$ ,  $b = \theta_6 - \theta_3$ ,  $a' = \theta_{300} + \theta_6$ ,  $b' = \theta_{600} + \theta_3$ ,  $c = \theta_{600} \times \theta_3$ ,  $d = \theta_{300} \times \theta_6$ , here  $\theta_3$ ,  $\theta_{300}$ ,  $\theta_{600}$  represent the rheological coefficients is in rotary viscometer’s rotor with rotation rate  $N_3 = 3$  r/min,  $N_{300} = 300$  r/min and  $N_{600} = 600$  r/min, respectively,  $\Delta P_h$  is the H-B mode fluid pressure difference at both sides of the pipe in the detection range:

$$\Delta P_h = \frac{2KL_A}{R} \left( \frac{3n + 1}{4n} \right)^n \left( \frac{4u}{R} \right)^n + \left( \frac{3n + 1}{2n + 1} \right) \frac{2\tau_0 L_A}{R}, \tag{25}$$

yield value  $\tau_0$ :

$$\tau_0 = 0.511 \frac{\theta_{600}\theta_3 - \theta_x^2}{C_1(\theta_{600} + \theta_3 - 2\theta_x)}, \quad (26)$$

$\theta_x = \tau_x/0.511$ , the coefficient  $C_1$ :

$$C_1 = \frac{1}{1-n} \frac{1 - (R_i/R_0)^{2/n-2}}{1 - (R_i/R_0)^{2/n}}, \quad (27)$$

$n$  is the liquidity index:

$$n = \frac{\lg[(\theta_{600} - \theta_x)/(\theta_x - \theta_3)]}{\lg(N_{600}/N_3)}, \quad (28)$$

$K$  is the viscosity coefficient:

$$K = \frac{1}{C_2} \frac{(\theta_{600} - \theta_3)}{(N_{600}^n - N_3^n)}, \quad (29)$$

coefficients  $C_2$ :

$$C_2 = \left\{ \frac{0.20944}{n[1 - (R_i/R_0)^{2/n}]} \right\}^n, \quad (30)$$

the flow core radius  $r_m$ :

$$r_m = \frac{2A\tau_0}{\Delta P_h}. \quad (31)$$

#### (5) Robertson–Stiff model [11]

R-S mode velocity distribution function  $v(r)_1$ :

$$v(r)_1 = \frac{B'}{B'+1} \left( \frac{\Delta P_l}{2A'L_A} \right)^{\frac{1}{B'}} (R^{\frac{B'+1}{B'}} - r^{\frac{B'+1}{B'}}) - C'(R-r). \quad (32)$$

where,  $\Delta P_l$  is the R-S mode fluid pressure difference at both sides of the pipe in the detection range:

$$\Delta P_l = \frac{2A'A}{R} \left[ \frac{3B+1}{B'R} \left( u + \frac{C'R}{3} \right) \right]^{B'}, \quad (33)$$

the viscosity coefficients  $A'$ :

$$A' = 0.511 \left[ \frac{B'(\theta_{600}^{1/B'} - \theta_x^{1/B'})(1 - 0.93646^{2/B'})}{0.20944(600 - N_x)} \right]^{B'}, \quad (34)$$

the liquidity index  $B'$ :

$$B' = \frac{\lg\left(\frac{\theta_{600}}{\theta_x}\right)}{\lg\left(\frac{600-N_x}{N_x-3}\right)}, \quad (35)$$

the shear rate correction value  $C'$ :

$$C' = \frac{B' \left(\frac{0.511\theta_{600}}{A}\right)^{1/B'} (1 - 0.93646^{2/B'}) - 125.664}{0.13128672}, \quad (36)$$

$N_x$  according to the  $\theta_x$ ,  $N_1$  and  $N_2$ :

$$N_x = N_1 + \frac{\tau_x - \tau_1}{\tau_2 - \tau_1} (N_2 - N_1), \quad (37)$$

R-S yield value  $\tau_x$ :

$$\tau_x = 0.511 \sqrt{\theta_{600}\theta_3}. \quad (38)$$

## References

1. G.R. Coats, L.Z. Xiao, M.G. Prammer, *NMR Logging Principles and Applications[M]* (Gulf Professional Publishing, Houston, 1999)
2. F. Casanova, J. Perlo, B. Blümich, *Single-Sided NMR* (Springer, New York, 2011)
3. G.A. Matzkanin, in *nondestructive characterization of materials*. ed. by P. Holler, V. Hauck, C.O. Rund, R.E. Green (Springer, Berlin, 1989)
4. J.R. Suryan, Proc. Indian Acad. Sci. Sect. A **33**, 107–111 (1951)
5. A. Caprihan, E. Fukushima, Phys. Rep. **198**, 195–235 (1990)
6. J.R. Singer, Science **130**(3389), 1652–1653 (2013)
7. F. Deng, L.Z. Xiao, H.B. Liu, T.L. An, M.Y. Wang, Z.F. Zhang, W. Xu, J.J. Cheng, Q.M. Xie, V. Anferov, Appl. Magn. Reson. **44**, 1053–1065 (2013)
8. E.C. Bingham, *Fluidity and Plasticity* (McGraw-Hill Book Co., New York 1922)
9. N. Casson, in *Rheology of Disperse Systems*, ed. by C.C. Mill (Pergamon Press, London, 1959), p. 84
10. W.H. Herschel, R. Bulkley, Proc. ASTM **26**(II), 621–633 (1926)
11. R.E. Robertson, Soc. Pet. Eng. J. **16**(1), 31–36 (1976)
12. G.R. Coats, L.Z. Xiao, M.G. Prammer, *NMR Logging Principles and Applications [M]* (Gulf Professional Publishing, Houston, 1999)
13. M.G. Prammer, J. Bouton, P. Masak. Magnetic resonance fluid analysis apparatus and method. US, 20020140425A1[P], 2002-10-03
14. B.S. Wu, L.Z. Xiao, X. Li, H.J. Yu, T.L. An, Pet. Sci. **9**(1), 38–45 (2012)
15. H.J. Yu, L.Z. Xiao, X. Li, H.B. Liu, B.X. Guo, S. Anferov, V. Anferov, in 2011 IEEE International Conference on Signal Processing, Communication and computing, ICSPCC 2011. 6061656
16. F. Deng, L.Z. Xiao, W.L. Chen, H.B. Liu, G.Z. Liao, M.Y. Wang, Q.M. Xie, J. Magn. Reson. **247**, 1–8 (2014)
17. F. Deng, L.Z. Xiao, G.Z. Liao, F.R. Zong, W.L. Chen, Appl. Magn. Reson. **45**, 179–192 (2014)
18. Y.Q. Song, L. Venkataramanan, M.D. Hürlimann et al.,  $T_1$ – $T_2$  correlation spectra obtained using a fast two-dimensional laplace inversion. J. Magn. Reson. **154**, 261–268 (2002)